Modeling Stator Winding Inter-Turn Short Circuit Faults in PMSMs including Cross Effects

Saeed Hasan Ebrahimi, Martin Choux, and Van Khang Huynh

Department of Engineering Sciences
University of Agder
NO-4879 Grimstad, Norway

Abstract – This paper presents a detailed analysis of stator winding inter-turn Short Circuit (ITSC) faults, taking the cross effects in the three phases of a permanent magnet synchronous motor (PMSM) into account by considering insulation degradation resistances. A PMSM with series coils in each phase winding is selected as a case study.The ITSC in one coil of each phase winding is modelled based on deformed fluxes or inductance variations caused by flux linkages, depending on the distribution of the coils in the same phase winding. Different fault ratios are investigated to evaluate different fault severity and scenarios. Therefore, three-phase faulty coils within three-phase winding analysis dynamics will constitute sixth-order assessments. The proposed faulty PMSM model is verified by a 2-D finite element analysis (FEA), showingc a good agreement between the proposed model and FEA.

B.1 Introduction

Permanent magnet synchronous motors (PMSMs) have gained a popularity in industry owing to their merits of high efficiency, high power density, and high reliability [1–3]. PMSMs often work in a harsh industrial environment and therefore, are exposed to electrical, thermal, and mechanical stresses. This creates the ground for different types of faults to appear, including electrical, mechanical, and magnetic faults [4]. Among the electrical faults, the stator winding inter-turn short circuit (ITSC) fault is considered as the most common fault [5], and at the same time, the most critical one due to the excessive heat generated by the high circulating fault current [6]. ITSC occurs with a few shorted turns in one coil due to the stator winding insulation failure. The insulation failure provides a degraded path between the shorted turns with a non-zero fault resistance, R_f, with a circulating fault current of i_f. This path causes unbalance in the magnetic field, generating excessive heat, which may propagate to the whole coil or other phases [7] if not being treated in time. Therefore, understating and detecting the ITSC fault in early stages are of great importance in reducing the costs and down-times caused by the complete machine failure.

Diagnosis of ITSC has gained a significant attention in both industry and academia via previous studies. The ITSC fault can be detected by current signal analysis (CSA) and zero-sequence voltage component (ZSVC) harmonic monitoring using signal processing or filtering techniques, such as Fourier transform [8], wavelet transform [9], and Kalman

filter [10]. These existing signal-based methods are very powerful to detect a fault but have some limitations on determining the fault severity, ITSC faults at different locations of the phase winding, or requiring external resistor network and neutral point of the stator windings [1, 2]. Alternatively, data-driven models, e.g using artificial neural network (ANN), were also proposed to detect or classify the faults. The data driven models are required a lot of historical faulty data for training to be robust and reliable [11]. In addition to signal-based and data-driven techniques, many model-based methods have intensively been employed to detect ITSC fault [12–14], but such models are hard to be applicable to multi-pole PMSMs since they ignore the flux coupling factor between healthy and faulty coils in the same phase winding. This coupling factor was well proposed and investigated in [15]. However, the cross effect of simultaneous fault currents in different phases is not modeled or still missing in literature. Modelling the interaction of one fault on other phases is important to understand the behaviour of magnetic flux and output characteristics of an unbalance PMSM under faults, being useful to develop a fault indicator in both steady and transient states. Although very unlikely for ITSC faults to appear in different phases at the same time, having a comprehensive model that detects and understands this phenomenon is very helpful when it comes to isolate faults in the machine diagnostic systems. Moreover, since the ITSC fault in one phase may propagate to other windings if not treated in time [16], adding this extra layer of fault detection when designing the sequence of faults, helps improve the performance and reliability of the diagnostic system.

The study presents an analytical model of a faulty PMSM considering simultaneous ITSC faults in each of the three-phase windings, in which the insulation degradation and the flux coupling between healthy and faulty coils in each phase are modeled as a resistance (R_f) and a factor (γ), respectively. Further, the cross-effect of fault currents in different phases is analysed by modified mutual inductances and coupling factor, allowing the modeling to be more comprehensive to understand the machine behaviors in a wide range of operations in different fault scenarios. The fault model is developed in a way to obtain deformed fluxes based on inductance variations caused by cross flux linkages, depending on the distribution of the coils in the same phase winding and cross-effects of fault currents in different phases. The remainder of the paper is organized as follows: modelling the ITSC fault in PMSM is detailed in Section II. Section III presents simulation results and a comparison with FEA. Finally, the paper is concluded in Section IV.

B.2 Modeling ITSC fault in the windings of PMSM

An 8-pole surface-mounted PMSM with concentrated winding is chosen as the case study for implementation of simultaneous ITSC faults in different phase windings. The reason that a concentrated winding structure is considered here, is simply because it is easier for this modeling to be implemented on. The same procedure can be applied on a motor with distributed winding with a few modifications in the flux equations. A 2D view of this PMSM is depicted in Fig. B.1 while motor parameters are listed in Table B.1. Some of these parameters are obtained from the manufacturer data-sheet and the rest from a few

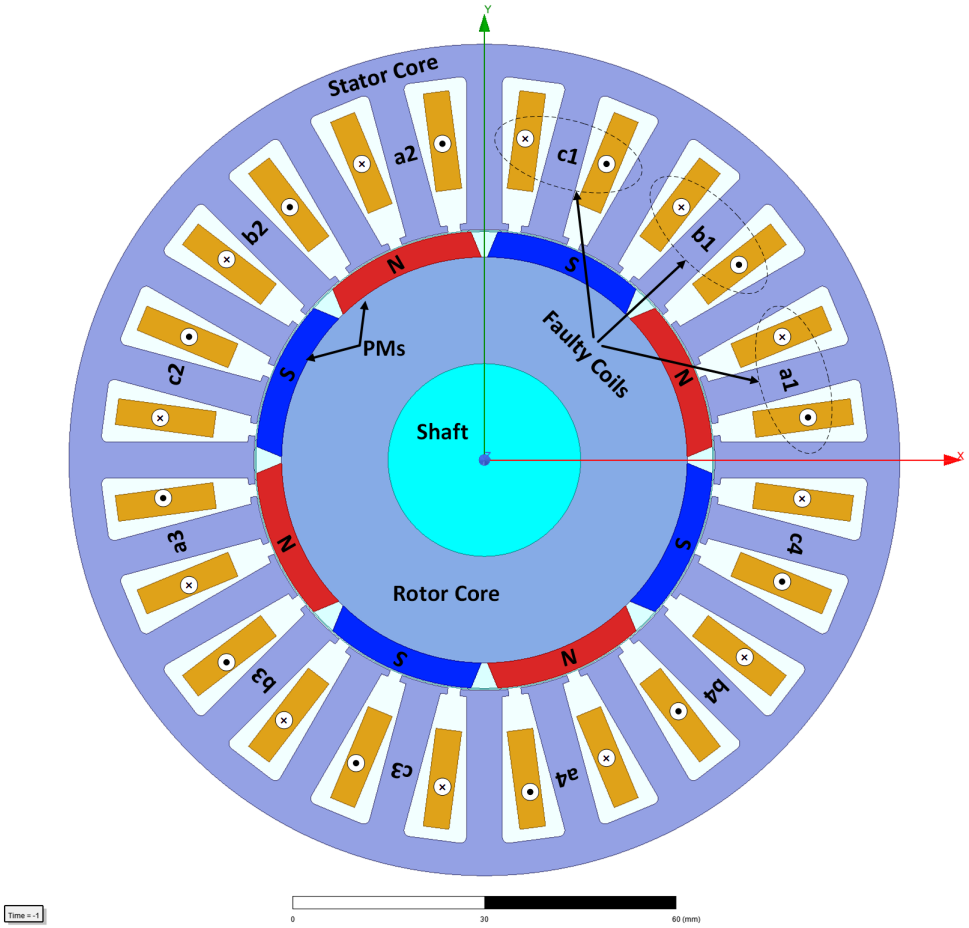

Figure B.1: 2D Structure of PM Synchronous Motor.

FEM Simulations which are explained in [15]. Each phase winding consists of 4 (number of pole-pairs) coils denoted by $a_{1,2,3,4}$, $b_{1,2,3,4}$, and $c_{1,2,3,4}$, which are connected in series. It is assumed that an ITSC fault is present in the first coils of each of the three-phase windings, splitting the coil into one faulty part and one healthy part. The fault severity $\mu_{a,b,c}$ is defined as the ratio of number of the shorted turns to the total number of turns per coil. In addition, the phase fault resistances and circulating fault currents in the degraded path are denoted by $R_{af,bf,cf}$ and $i_{af,bf,cf}$, respectively. Fig. B.2 shows the schematic of winding configuration of series connection under three simultaneous faults in the three phases.

Modeling flux linkages between different coils was first proposed by [15],considering the interaction between the faulty part and healthy part of the same coil with other healthy coils in the same winding. This interaction is considered in the modeling with a coupling factor γ, and is especially important in PMSMs with multiple pole pairs ($p > 1$), where the flux linkages between coils in the same phase winding are affected by many possible flux paths. However, the suggested method is only valid for ITSC in one phase. To extend and generalize the concept for other phases, cross effect of ITSC faults in different phases are modelled in this work.

Table B.1: Parameters of PM Synchronous Motor

Symbol	Parameter	Value	Unit
V_s	Rated line voltage	320	V
I_s	Rated phase current	12.6	A
T_{out}	Output Torque	14	$N.m$
n_s	Rated speed	1200	rpm
R_s	Phase resistance	1.72	Ω
L_s	Phase leakage inductance	16.3652	mH
L_q, L_d	Q and D axes inductances	23.3948	mH
J	Rotor inertia	0.00161	$kg.m^2$
b	Rotor damping factor	0.002973	$N.m.s/rad$
λ_m	Flux linkage of PMs	0.1722	
γ	Winding coupling factor	0.6	
n_s	Number of Slots	24	

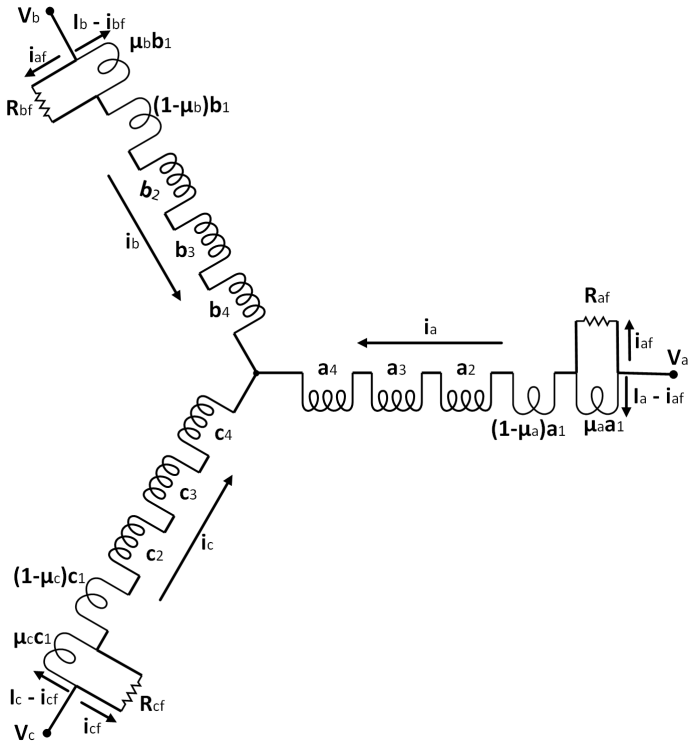

Figure B.2: Winding configuration with series connected coils under a 3-phase ITSC fault.

B.2.1 Deformed Flux-Current Equations of PMSM with ITSC

Taking the effects of simultaneous faults in different phases into account, the flux-current equations for faulty and healthy parts of the stator windings are obtained as follows [15]:

$$\begin{bmatrix}\lambda_{af}\\ \lambda_{ah}\\ \lambda_{bf}\\ \lambda_{bh}\\ \lambda_{cf}\\ \lambda_{ch}\end{bmatrix} = \begin{bmatrix} L_{a_fa_f} & L_{a_fa_h} & L_{a_fb_f} & L_{a_fb_h} & L_{a_fc_f} & L_{a_fc_h}\\ L_{a_ha_f} & L_{a_ha_h} & L_{a_hb_f} & L_{a_hb_h} & L_{a_hc_f} & L_{a_hc_h}\\ L_{b_fa_f} & L_{b_fa_h} & L_{b_fb_f} & L_{b_fb_h} & L_{b_fc_f} & L_{b_fc_h}\\ L_{b_ha_f} & L_{b_ha_h} & L_{b_hb_f} & L_{b_hb_h} & L_{b_hc_f} & L_{b_hc_h}\\ L_{c_fa_f} & L_{c_fa_h} & L_{c_fb_f} & L_{c_fb_h} & L_{c_fc_f} & L_{c_fc_h}\\ L_{c_ha_f} & L_{c_ha_h} & L_{c_hb_f} & L_{c_hb_h} & L_{c_hc_f} & L_{c_hc_h}\end{bmatrix} \begin{bmatrix} i_{af}\\ i_a - i_{af}\\ i_{bf}\\ i_b - i_{bf}\\ i_{cf}\\ i_c - i_{cf}\end{bmatrix} + \begin{bmatrix} \mu_a \sin\theta\\ (1-\mu_a)\sin\theta\\ \mu_b \sin(\theta - \frac{2\pi}{3})\\ (1-\mu_b)\sin(\theta - \frac{2\pi}{3})\\ \mu_c \sin(\theta + \frac{2\pi}{3})\\ (1-\mu_c)\sin(\theta + \frac{2\pi}{3})\end{bmatrix} \tag{B.1}$$

where the self and mutual inductances are modified as below

$$\begin{aligned}
L_{a_fa_f} &= \mu_a^2(L_{sl} + L_{sm})\\
L_{a_fa_h} &= L_{a_ha_f} = -\gamma\mu_a L_{sm} + \mu_a(1-\mu_a)(L_{sl} + L_{sm})\\
L_{a_ha_h} &= [p - 1 + (1-\mu_a)^2](L_{sl} + L_{sm}) - \gamma\mu_a L_{sm}(p - 2\mu_a)\\
L_{b_fb_f} &= \mu_b^2(L_{sl} + L_{sm})\\
L_{b_fb_h} &= L_{b_hb_f} = -\gamma\mu_b L_{sm} + \mu_b(1-\mu_b)(L_{sl} + L_{sm})\\
L_{b_hb_h} &= [p - 1 + (1-\mu_b)^2](L_{sl} + L_{sm}) - \gamma\mu_b L_{sm}(p - 2\mu_b)\\
L_{c_fc_f} &= \mu_c^2(L_{sl} + L_{sm})\\
L_{c_fc_h} &= L_{c_hc_f} = -\gamma\mu_c L_{sm} + \mu_c(1-\mu_c)(L_{sl} + L_{sm})\\
L_{c_hc_h} &= [p - 1 + (1-\mu_c)^2](L_{sl} + L_{sm}) - \gamma\mu_c L_{sm}(p - 2\mu_c)\\
L_{a_fb_f} &= L_{b_fa_f} = -\mu_a\mu_b\frac{L_m}{2p^2}\\
L_{a_fb_h} &= L_{b_ha_f} = -\frac{L_m}{2p^2}\mu_a(p - \mu_b)\\
L_{a_hb_f} &= L_{b_fa_h} = -\frac{L_m}{2p^2}\mu_b(p - \mu_a)\\
L_{a_hb_h} &= L_{b_ha_h} = -\frac{L_m}{2p^2}[p^2 - p(\mu_a + \mu_b) + \mu_a\mu_b]\\
L_{a_fc_f} &= L_{c_fa_f} = -\mu_a\mu_c\frac{L_m}{2p^2}\\
L_{a_fc_h} &= L_{c_ha_f} = -\frac{L_m}{2p^2}\mu_a(p - \mu_c)\\
L_{a_hc_f} &= L_{c_fa_h} = -\frac{L_m}{2p^2}\mu_c(p - \mu_a)\\
L_{a_hc_h} &= L_{c_ha_h} = -\frac{L_m}{2p^2}[p^2 - p(\mu_a + \mu_c) + \mu_a\mu_c]
\end{aligned} \tag{B.2}$$

$$
\begin{aligned}
L_{b_f c_f} &= L_{c_f b_f} = -\mu_b \mu_c \frac{L_m}{2p^2} \\
L_{b_f c_h} &= L_{c_h b_f} = -\frac{L_m}{2p^2} \mu_b (p - \mu_c) \\
L_{b_h c_f} &= L_{c_f b_h} = -\frac{L_m}{2p^2} \mu_c (p - \mu_b) \\
L_{b_h c_h} &= L_{c_h b_h} = -\frac{L_m}{2p^2} [p^2 - p(\mu_b + \mu_c) + \mu_b \mu_c]
\end{aligned}
$$

B.2.2 Modelling PMSM under 3-phase ITSC faults

Stator voltage of a synchronous motor in the stationary frame is obtained as follows:

$$
v_s = r_s i_s + \frac{d\lambda_s}{dt} \tag{B.3}
$$

where

$$
\begin{aligned}
v_s &= \begin{bmatrix} v_{af} & v_{ah} & v_{bf} & v_{bh} & v_{cf} & v_{ch} \end{bmatrix}^T \\
i_s &= \begin{bmatrix} i_{af} & i_a - i_{af} & i_{bf} & i_b - i_{bf} & i_{cf} & i_c - i_{cf} \end{bmatrix}^T \\
r_s &= R_s diag \begin{bmatrix} \mu_a & 1-\mu_a & \mu_b & 1-\mu_b & \mu_c & 1-\mu_c \end{bmatrix}^T
\end{aligned}
$$

By summing up the voltages of faulty and healthy parts in each phase using Eq. B.3, and considering phase winding linkage and leakage inductances to be $L_{sm} = L_m/p(1-\gamma)$ and $L_{sl} = L_l/p$, respectively, the three-phase voltage-current equations of the PMSM under ITSC fault are derived as follows:

$$
\begin{aligned}
&\begin{bmatrix} v_a \\ v_b \\ v_c \end{bmatrix} = R_s \begin{bmatrix} i_a \\ i_b \\ i_c \end{bmatrix} + \begin{bmatrix} L_m + L_l & -\frac{L_m}{2} & -\frac{L_m}{2} \\ -\frac{L_m}{2} & L_m + L_l & -\frac{L_m}{2} \\ -\frac{L_m}{2} & -\frac{L_m}{2} & L_m + L_l \end{bmatrix} \begin{bmatrix} \frac{di_a}{dt} \\ \frac{di_b}{dt} \\ \frac{di_c}{dt} \end{bmatrix} \\
&+ \omega_e \lambda_m \begin{bmatrix} \cos\theta \\ \cos(\theta - \frac{2\pi}{3}) \\ \cos(\theta + \frac{2\pi}{3}) \end{bmatrix} - \frac{R_s}{p} \begin{bmatrix} \mu_a & 0 & 0 \\ 0 & \mu_b & 0 \\ 0 & 0 & \mu_c \end{bmatrix} \begin{bmatrix} i_a \\ i_b \\ i_c \end{bmatrix} \\
&- \frac{1}{p} \begin{bmatrix} L_m + L_l & -\frac{L_m}{2} & -\frac{L_m}{2} \\ -\frac{L_m}{2} & L_m + L_l & -\frac{L_m}{2} \\ -\frac{L_m}{2} & -\frac{L_m}{2} & L_m + L_l \end{bmatrix} \begin{bmatrix} \mu_a & 0 & 0 \\ 0 & \mu_b & 0 \\ 0 & 0 & \mu_c \end{bmatrix} \begin{bmatrix} \frac{di_a}{dt} \\ \frac{di_b}{dt} \\ \frac{di_c}{dt} \end{bmatrix}
\end{aligned} \tag{B.4}
$$

By assuming that $v_{af} = R_{af} i_{af}$,$v_{bf} = R_{bf} i_{bf}$, and $v_{cf} = R_{cf} i_{cf}$ and using Eq. B.3 and Eq. B.4, the fault currents can be derived from:

$$
\begin{aligned}
v_a &= [\frac{pR_{af}}{\mu_a} + R_s(1 - \frac{\mu_a}{p})] i_{af} + \frac{\mu_a}{p} [L_m(\frac{p - 1 + \gamma}{1 - \gamma}) + L_l(p-1)] \frac{di_a}{dt} \\
v_b &= [\frac{pR_{bf}}{\mu_b} + R_s(1 - \frac{\mu_b}{p})] i_{bf} + \frac{\mu_b}{p} [L_m(\frac{p - 1 + \gamma}{1 - \gamma}) + L_l(p-1)] \frac{di_b}{dt} \\
v_c &= [\frac{pR_{cf}}{\mu_c} + R_s(1 - \frac{\mu_c}{p})] i_{ac} + \frac{\mu_c}{p} [L_m(\frac{p - 1 + \gamma}{1 - \gamma}) + L_l(p-1)] \frac{di_c}{dt}
\end{aligned} \tag{B.5}
$$

B.2.3 Performance of PMSM under a ITSC

Using Eq. B.4, the input power of the PMSM is calculated as follows:

$$P_{in} = v_a i_a + v_b i_b + v_c i_c \tag{B.6}$$

After putting aside the terms that contribute to copper losses or stored magnetic energy in Eq. B.7, the output power is extracted as:

$$P_{out} = \omega_e \lambda_m [\cos\theta i_a + \cos(\theta - \frac{2\pi}{3}) i_b + \cos(\theta + \frac{2\pi}{3}) i_c] \tag{B.7}$$

And the output torque can be calculated as:

$$T_{out} = \frac{P_{out}}{\omega_m} = \frac{P_{out}}{\frac{1}{p}\omega_e} = \lambda_m [\cos\theta i_a + \cos(\theta - \frac{2\pi}{3}) i_b + \cos(\theta + \frac{2\pi}{3}) i_c] \tag{B.8}$$

B.3 Simulations and Results

To verify the proposed model, FEA of the PMSM is performed using Ansys-Maxwell. Four different cases including healthy condition, single ITSC fault in phase-a, simultaneous ITSC faults in phase-b and phase-c, and simultaneous ITSC faults in phase-a, phase-b and phase-c are tested to check the accuracy of the proposed model. Output torque, angular speed, three-phase currents, and fault currents characteristics are obtained. Although the proposed model is based on the three-phase currents and three-phase voltages monitoring, other output characteristics including torque and speed are demonstrated just for comparison. For analyzing incipient faults, the fault resistances are considered to be $R_{af,bf,cf} = 0.1\Omega$. Because the ITSC starts with a high degraded path resistance and as the fault grows the degraded path resistance value approaches zero. Further, to eliminate the effects of the drive system and switching noise on the performance of the motor, it is assumed that the motor is fed by a three-phase sinusoidal voltage source.

Fig. B.3 shows the comparison of motor's torque and speed obtained from the proposed model and FEA. It can be seen that even though a bit deviation in the transient part, the produced torque and speed from the proposed model match well those from FEA in. It is worth mentioning that the slot-effect was not investigated in the proposed model and that is the reason of the major difference in the proposed model and FEA results. However, this can be neglected as the produced results are close to the average values of FEA in the steady state. Fig. B.4 shows the comparison of motor's three-phase currents obtained from the proposed model and FEA. Since there is not any faults in the motor, the proposed model three-phase currents match those obtained from FEA.

Fig. B.5 shows the comparison of motor's torque and speed when the motor is experiencing one single ITSC fault in phase-a with 31 shorted turns (out of 71 total turns) and therefore, $\mu_a = 0.4366$, $\mu_b = 0$, and $\mu_c = 0$. It can be seen that ITSC fault creates some distortions in both torque and speed characteristics compared to the healthy condition.

Fig. B.6 shows the comparison of motor's three-phase currents obtained from the proposed model and FEA in this faulty scenario. The ITSC fault in phase-a has caused the phase-a current to be higher than two other phase currents. Fig. B.7 shows the

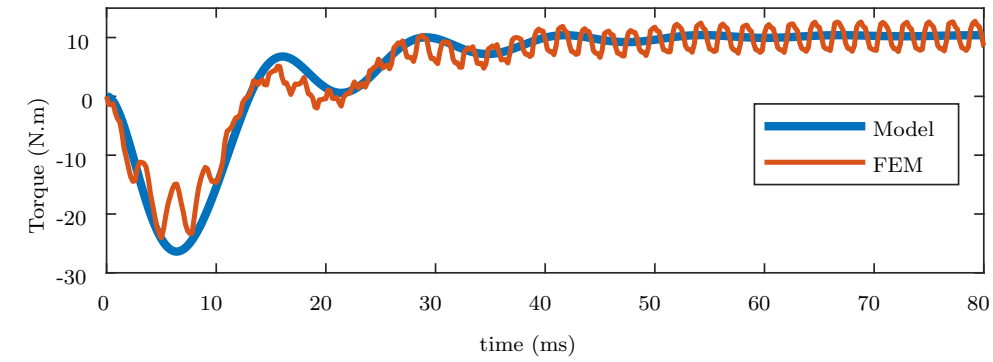

(a)

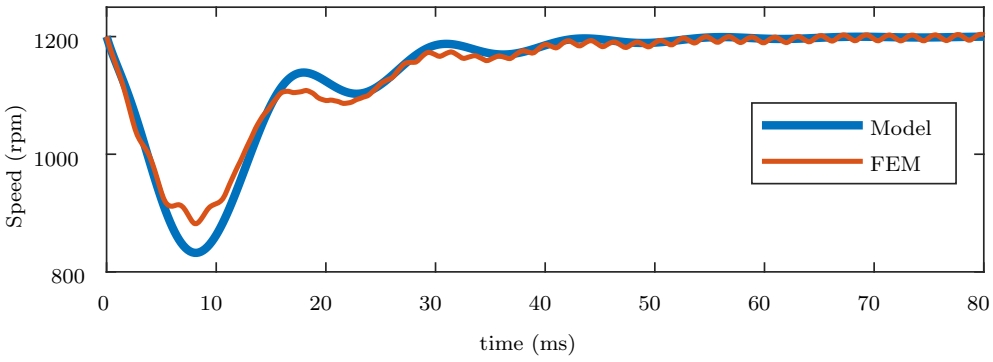

(b)

Figure B.3: (a) Output torque, (b) Motor speed, under healthy condition

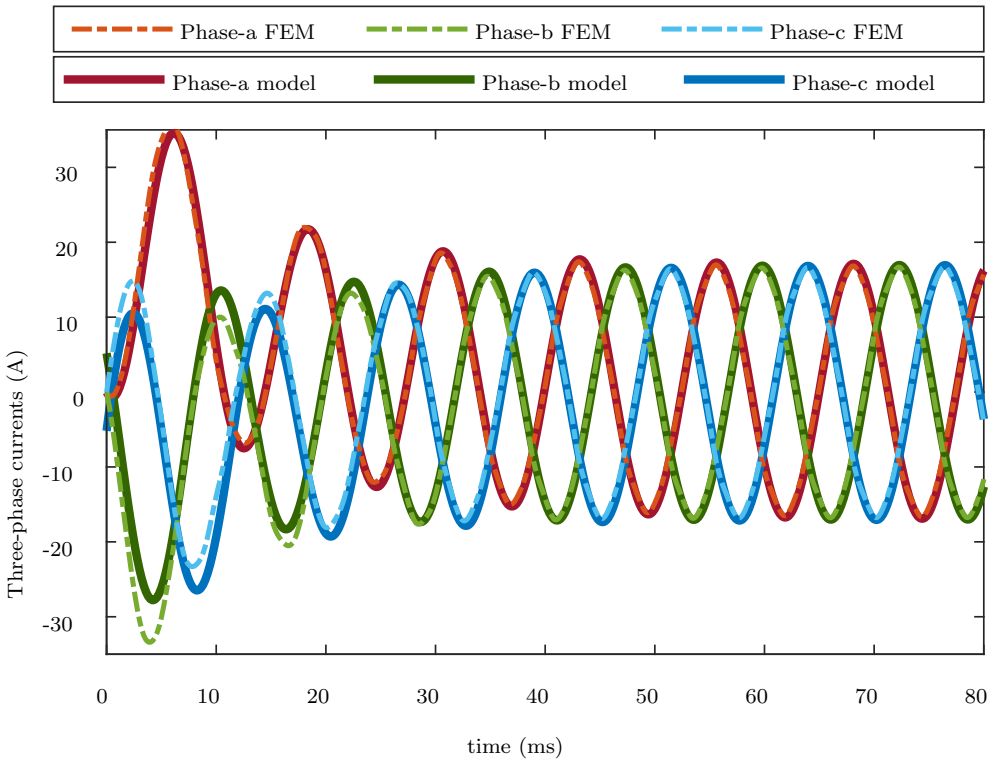

Figure B.4: Three-phase currents under healthy condition

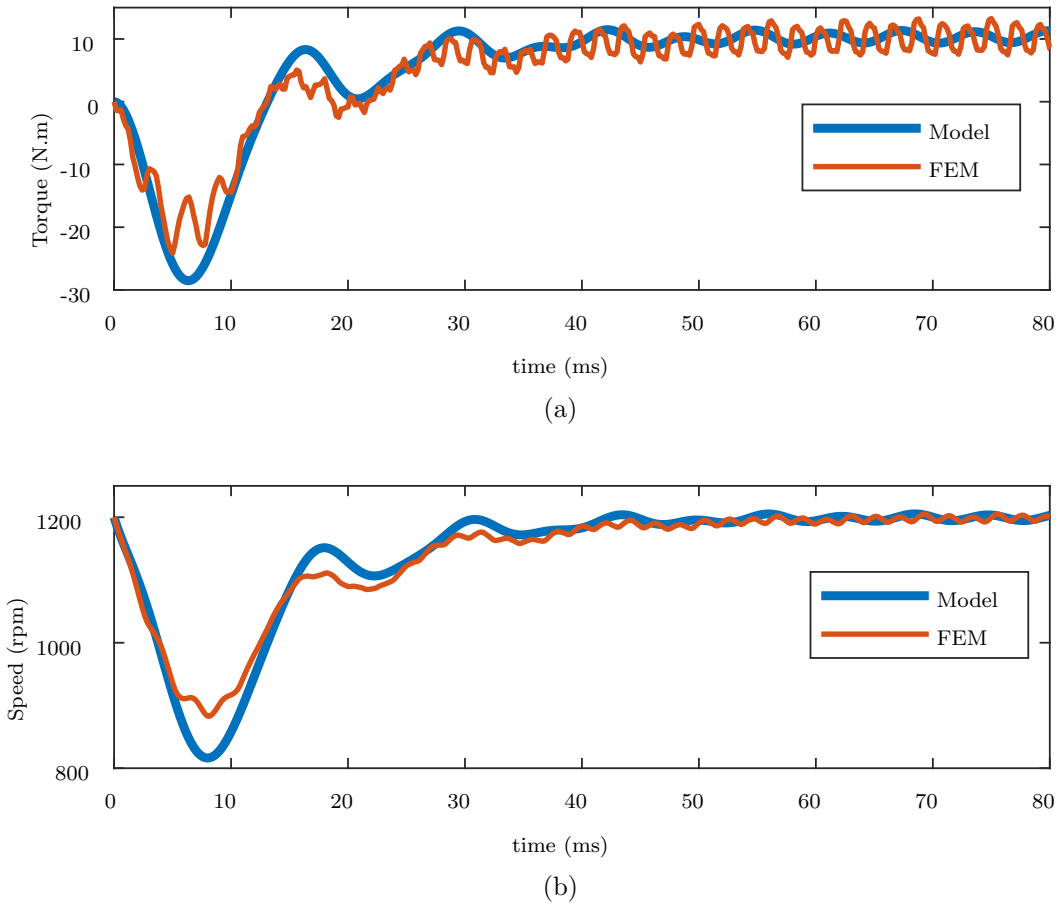

Figure B.5: (a) Output torque, (b) Motor speed, under $\mu_a = 0.4366$

comparison of motor's fault currents obtained from the proposed model and FEA. In this case, phase-b and phase-c fault currents are zero since there is not any faulty parts in these windings, but phase-a contains a fault current circulating in the faulty part of its winding.

Figs. B.8 shows the comparison of motor's torque and speed when the motor is operating under two simultaneous ITSC faults in phase-b with 40 shorted turns and phase-c with 20 shorted turns (out of 71 total turns) and therefore, $\mu_a = 0$, $\mu_b = 0.5634$, and $\mu_c = 0.2617$. The distortions in torque and speed characteristics are also present in this case due to unbalance caused by two faulty coils.

Fig. B.9 shows the comparison of motor's three-phase currents obtained from the proposed model and FEA in this case. The ITSC faults in phase-b and phase-c have caused the currents to be higher than phase-a current. Fig. B.10 shows the comparison of motor's fault currents obtained from the proposed model and FEA. In this case, phase-a fault current is zero since there is not any shorted turns in this windings, but phase-b and phase-c contain fault currents circulating in the faulty part of their windings.

Fig. B.11 shows the comparison of motor's torque and speed when the motor is experiencing three simultaneous ITSC faults in phase-a with 31 shorted turns, phase-b with 40 shorted turns, and phase-c with 20 shorted turns (out of 71 total turns) or $\mu_a = 0.4366$, $\mu_b = 0.5634$, and $\mu_c = 0.2617$. The level of distortions in both torque and speed charac-

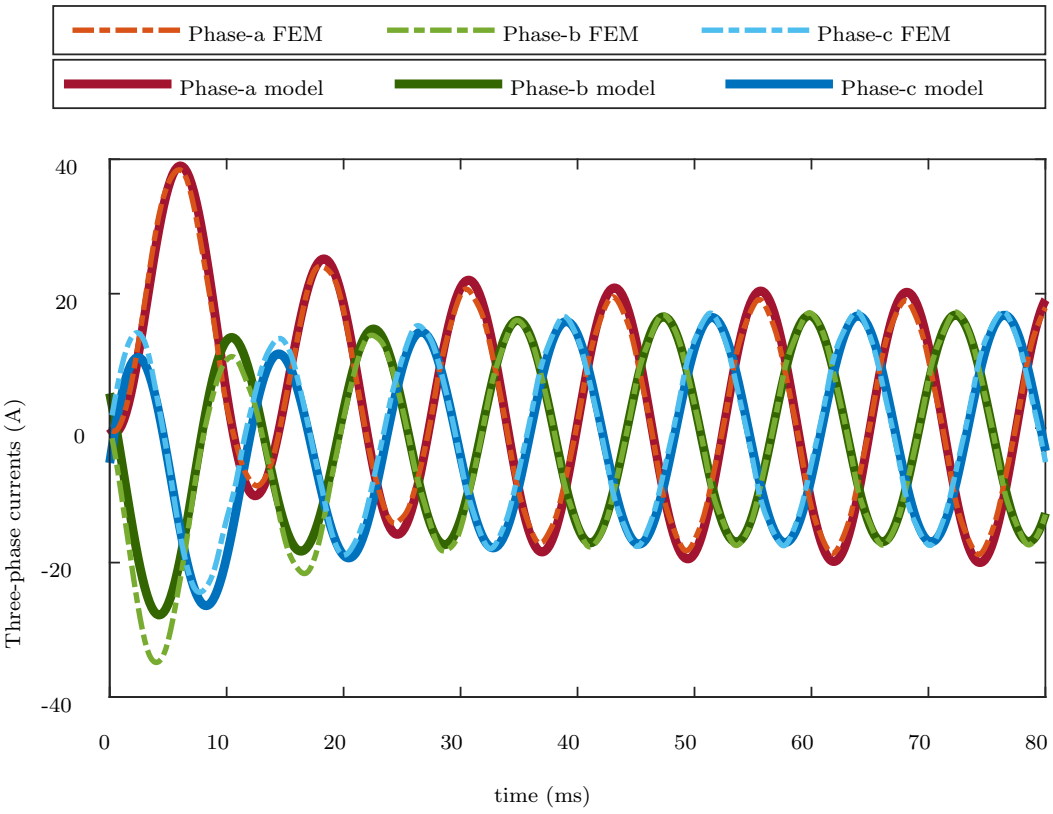

Figure B.6: Three-phase currents under $\mu_a = 0.4366$

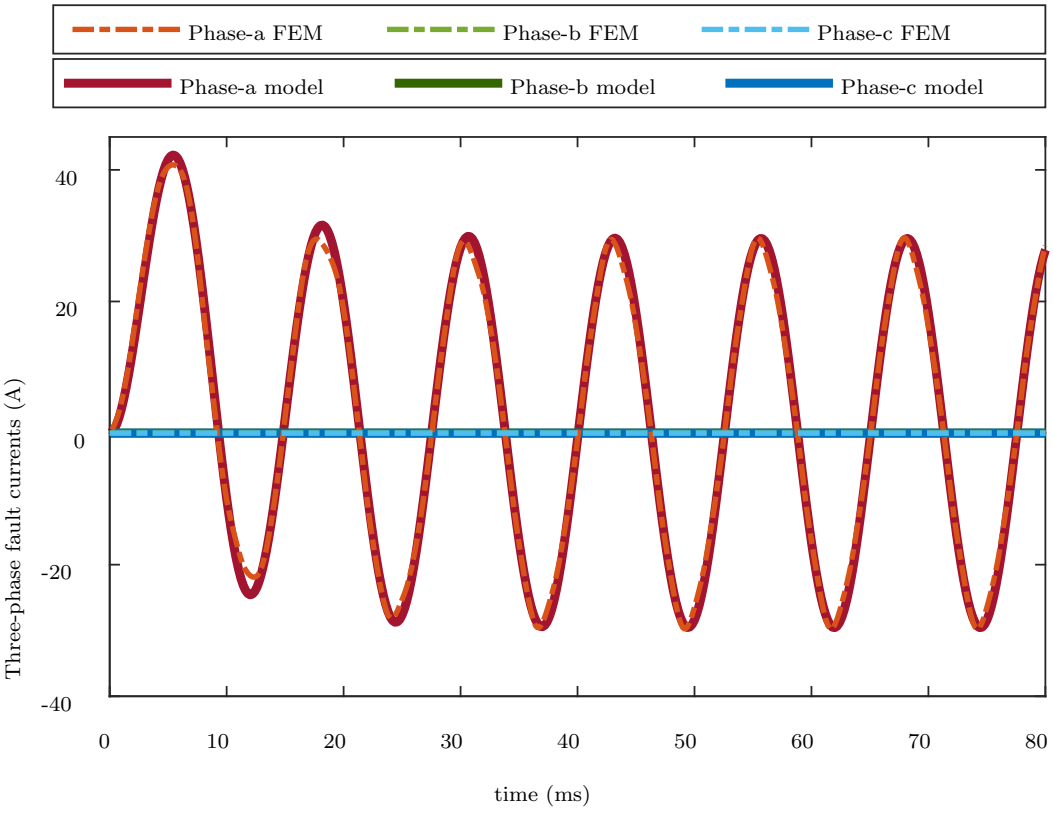

Figure B.7: Three-phase fault currents under $\mu_a = 0.4366$

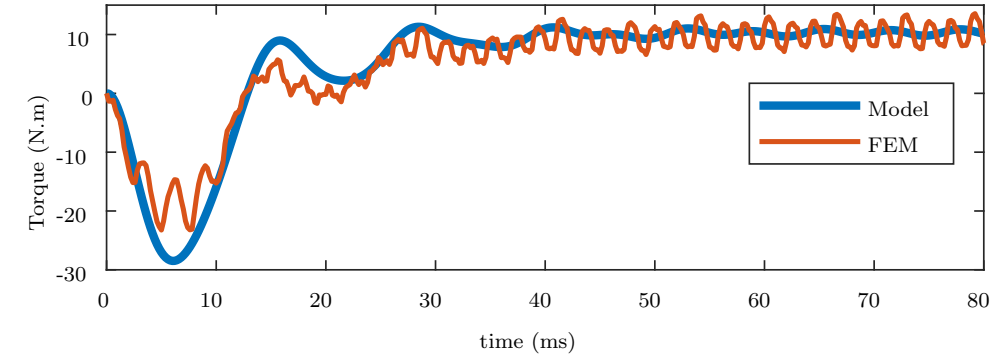

(a)

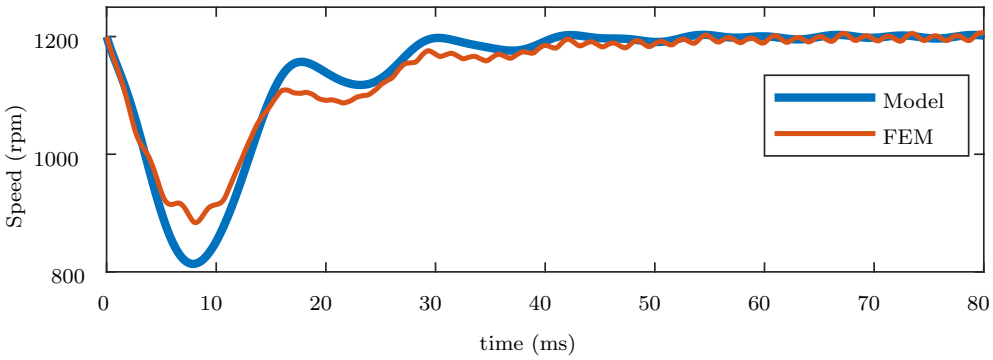

(b)

Figure B.8: (a) Output torque, (b) Motor speed, under $\mu_b = 0.5634$, and $\mu_c = 0.2617$

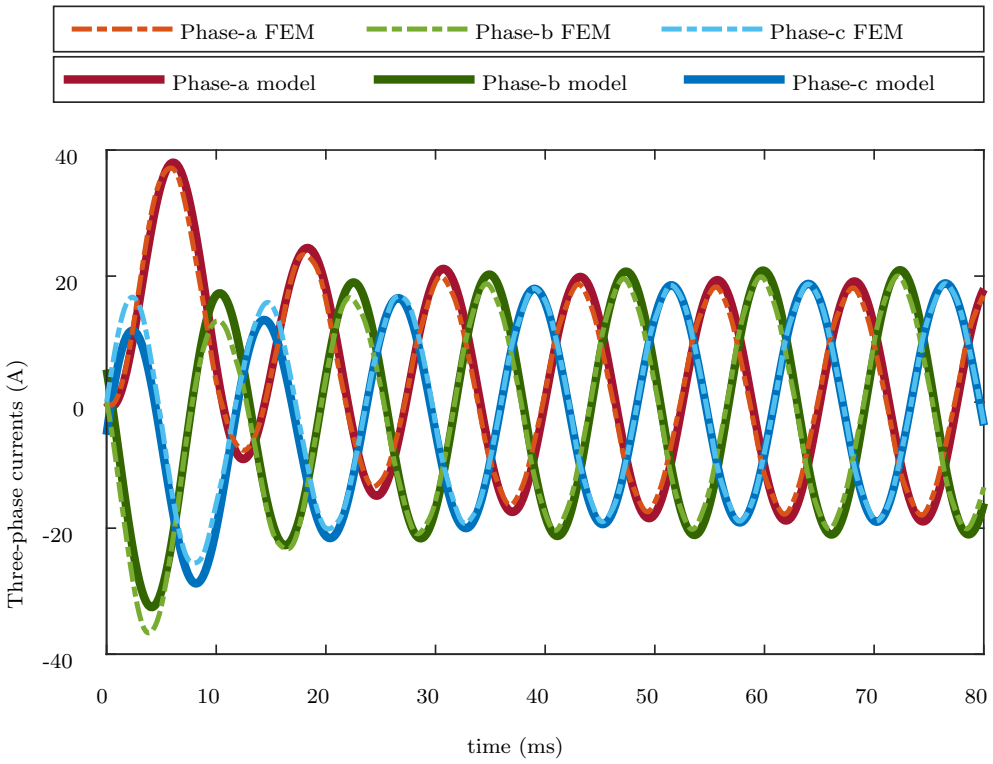

Figure B.9: Three-phase currents under $\mu_b = 0.5634$, and $\mu_c = 0.2617$

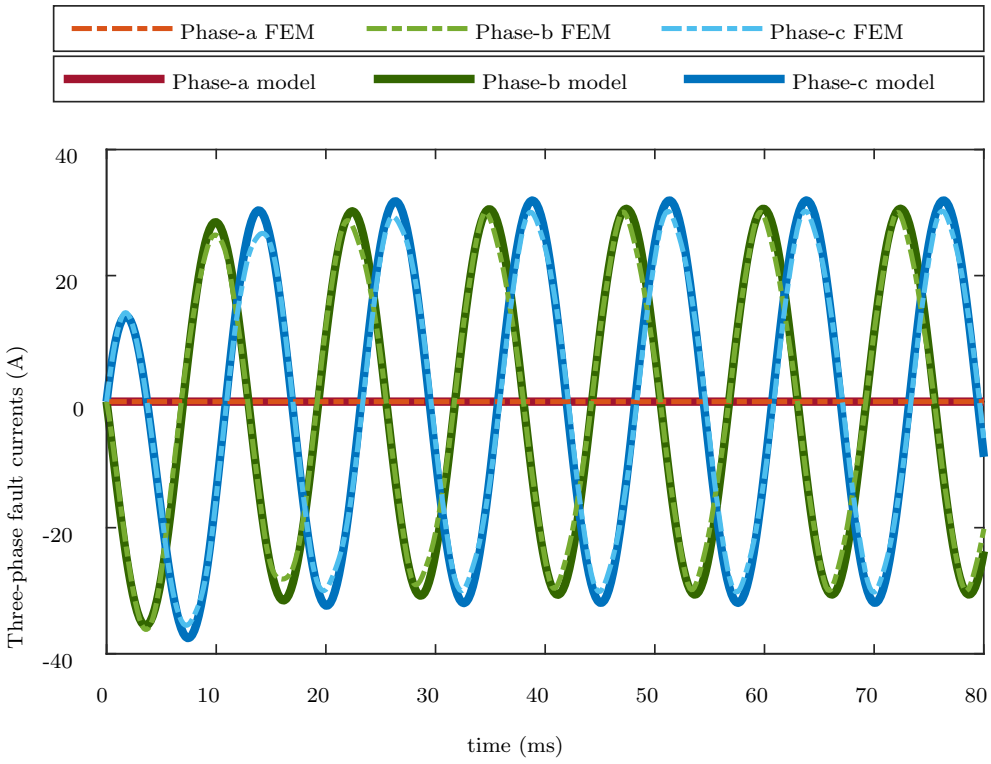

Figure B.10: Three-phase fault currents under $\mu_b = 0.5634$, and $\mu_c = 0.2617$

teristics are a bit decreased in this case compared to previous cases due to balance created by three faulty coils or three-phase fault currents.

Fig. B.12 shows the comparison of motor's three-phase currents obtained from the proposed model and FEA in this case. The ITSC faults in each phase have caused the currents to be higher compared to the healthy condition. Fig. B.13 shows the comparison of motor's fault currents obtained from the proposed model and FEA. In this case, all phases contain fault currents circulating in the faulty part of their windings. Similar to previous cases, there is an acceptable agreement between the proposed model and FEA results in the steady state although there are errors in the transient parts. Moreover, the cross-effects of simultaneous faults are well defined in the proposed model, which allow the model results to match the FEM results.

Fig. B.14 shows the comparison of motor's steady-state torque characteristics in different fault scenarios. It is obvious that motor's behavior is different under each case and this is majorly caused by different amplitudes and phases of current signals in each scenario. In addition, a single ITSC fault (case-1) creates more unbalance compared to two simultaneous ITSC faults (case-2) or three simultaneous ITSC faults (case-3), due to the higher generated negative sequence. This comparison also helps to understand the level of severity and potential damage that each case may have to the motor based on the mechanical stress caused by electromagnetic torque.

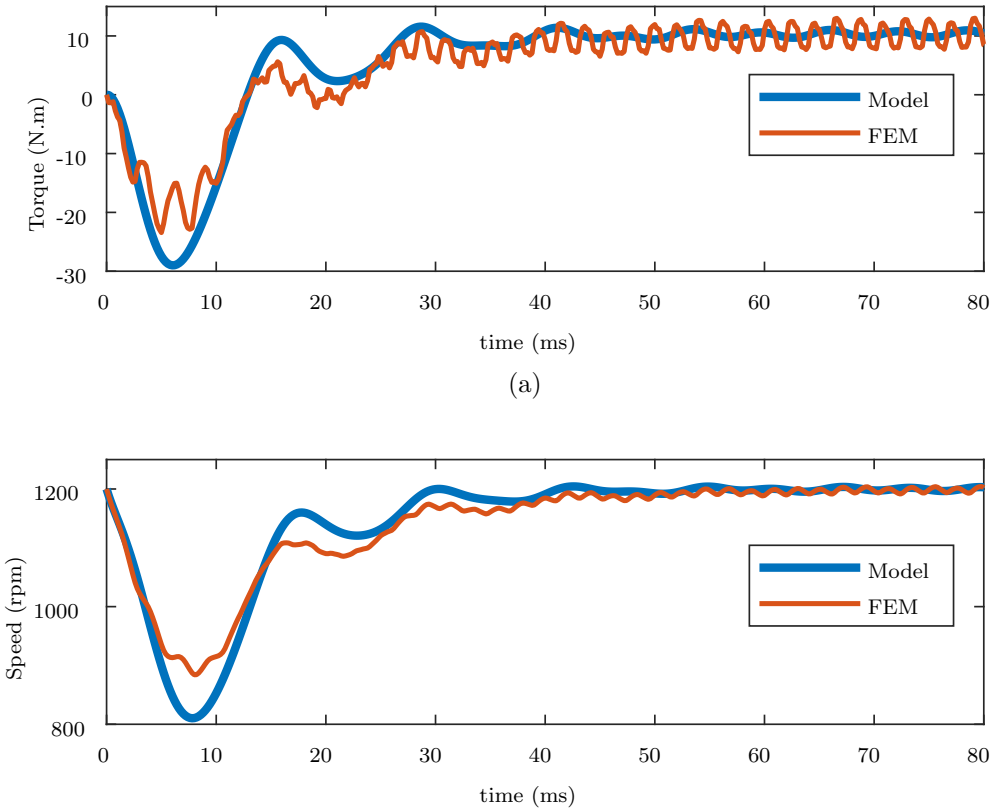

Figure B.11: (a) Output torque, (b) Motor speed, under $\mu_a = 0.4366$, $\mu_b = 0.5634$, and $\mu_c = 0.2617$

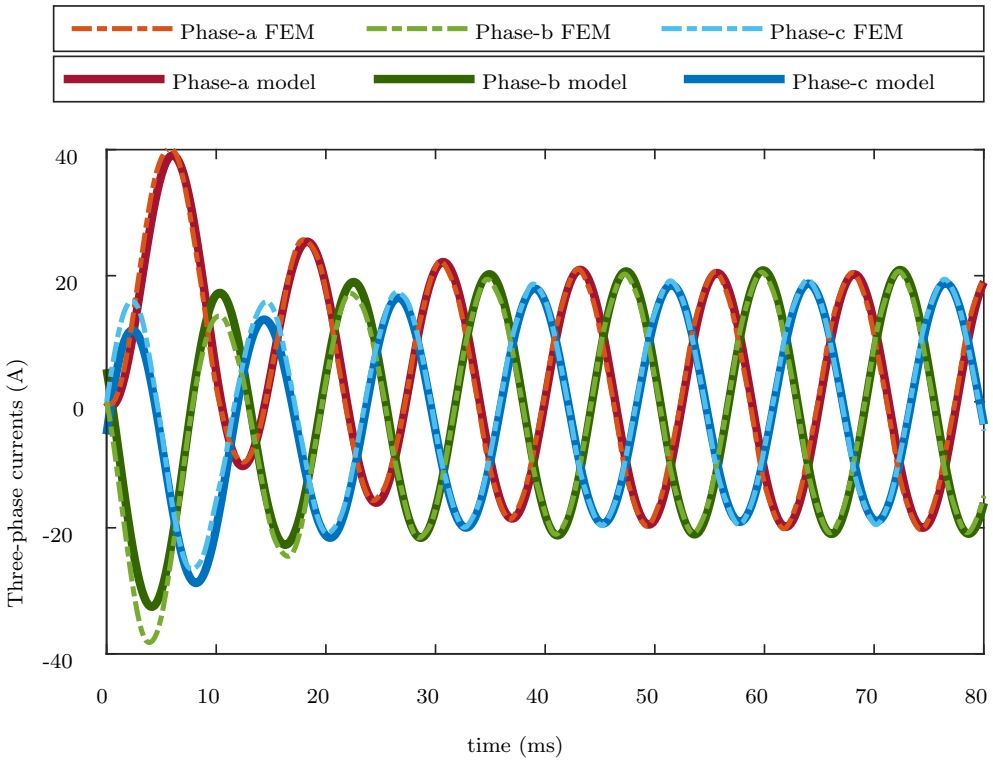

Figure B.12: Three-phase currents under $\mu_a = 0.4366$, $\mu_b = 0.5634$, and $\mu_c = 0.2617$

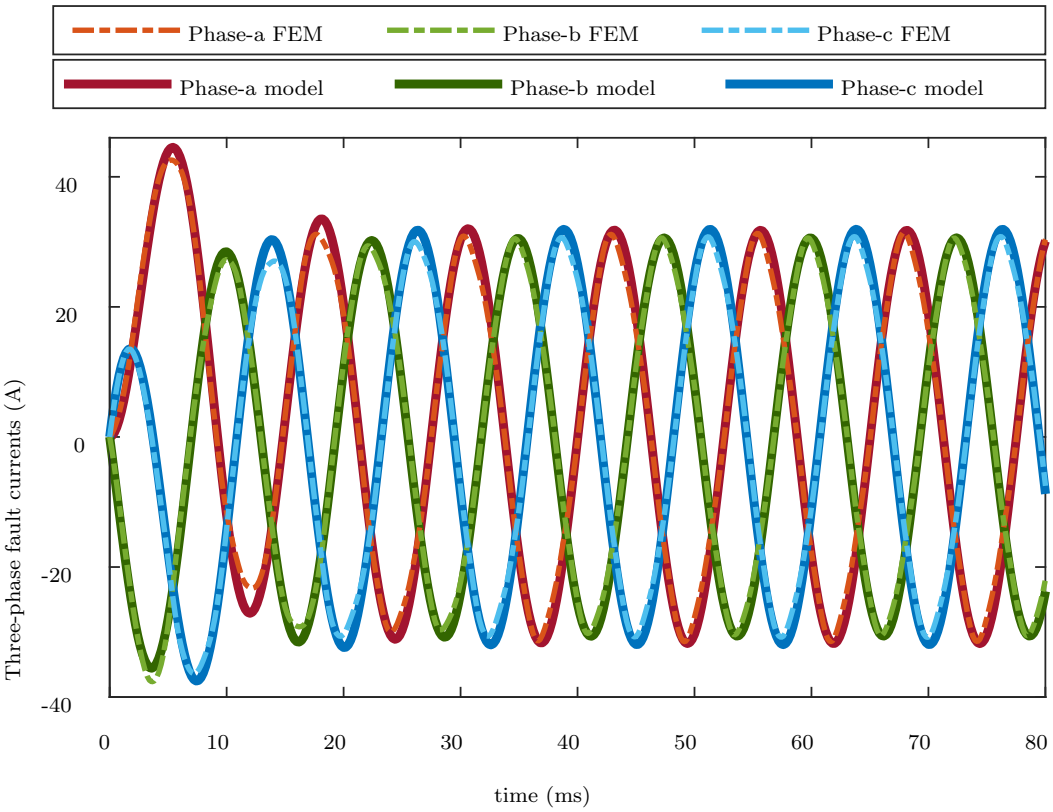

Figure B.13: Three-phase fault currents under $\mu_a = 0.4366$, $\mu_b = 0.5634$, and $\mu_c = 0.2617$

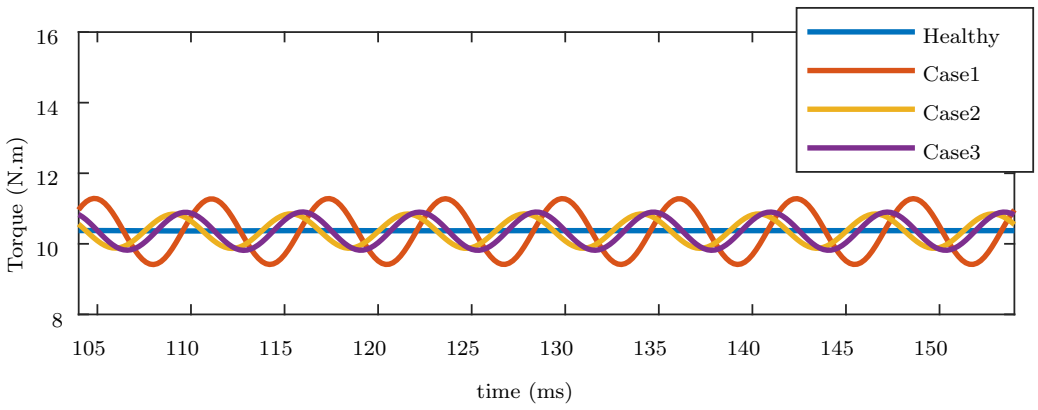

Figure B.14: Comparison of output torque in different cases.

B.4 Conclusion

In this paper, we presented a detailed modeling of ITSC faults in the PMSM. To accomplish this, a fault model was developed to obtain deformed fluxes based on inductance variations, which are caused by cross flux linkages depending on the distribution of the coils in the same phase winding. In addition, the cross-effect of fault currents in different phases was modeled, enabling the model to model not only single faults, but also simultaneous ITSC faults in any of the phases. The fault model requires only three-phase currents, three-phase voltages, and parameters of the motor as input. A time-stepping FEA was implemented to validate the results obtained from the proposed faulty PMSM model. Unlike FEA, the presented dynamic model can well and quickly model the behaviour of PMSM under different fault scenarios, without using detailed dimensions or material information. This allows developing fault indicators or detection methods in future studies.

References

[1] Seungdeog Choi, Moinul Shahidul Haque, Md Tawhid Bin Tarek, Vamsi Mulpuri, Yao Duan, Sanjoy Das, Vijay Garg, Dan M Ionel, M Abul Masrur, Behrooz Mirafzal, et al. Fault diagnosis techniques for permanent magnet ac machine and drives—a review of current state of the art. *IEEE Transactions on Transportation Electrification*, 4(2):444–463, 2018.

[2] Seokbae Moon, Hyeyun Jeong, Hojin Lee, and Sang Woo Kim. Interturn short fault diagnosis in a pmsm by voltage and current residual analysis with the faulty winding model. *IEEE Transactions on Energy Conversion*, 33(1):190–198, 2017.

[3] Richard T Meyer, Raymond A DeCarlo, Scott C Johnson, and Steve Pekarek. Short-circuit fault detection observer design in a pmsm. *IEEE Transactions on Aerospace and Electronic Systems*, 54(6):3004–3017, 2018.

[4] Bashir Mahdi Ebrahimi, Mehrsan Javan Roshtkhari, Jawad Faiz, and Seyed Vahid Khatami. Advanced eccentricity fault recognition in permanent magnet synchronous motors using stator current signature analysis. *IEEE Transactions on Industrial Electronics*, 61(4):2041–2052, 2013.

[5] Mohamed A Awadallah, Medhat M Morcos, Suresh Gopalakrishnan, and Thomas W Nehl. Detection of stator short circuits in vsi-fed brushless dc motors using wavelet transform. *IEEE Transactions on Energy Conversion*, 21(1):1–8, 2006.

[6] Sergio MA Cruz and AJ Marques Cardoso. Multiple reference frames theory: A new method for the diagnosis of stator faults in three-phase induction motors. *IEEE Transactions on Energy Conversion*, 20(3):611–619, 2005.

[7] Babak Vaseghi, Babak Nahid-Mobarakh, Noureddine Takorabet, and Farid Meibody-Tabar. Inductance identification and study of pm motor with winding turn short circuit fault. *IEEE Transactions on Magnetics*, 47(5):978–981, 2011.

[8] Bashir Mahdi Ebrahimi and Jawad Faiz. Feature extraction for short-circuit fault detection in permanent-magnet synchronous motors using stator-current monitoring. *IEEE Transactions on Power Electronics*, 25(10):2673–2682, 2010.

[9] Jeevanand Seshadrinath, Bhim Singh, and Bijaya Ketan Panigrahi. Investigation of vibration signatures for multiple fault diagnosis in variable frequency drives using complex wavelets. *IEEE Transactions on Power Electronics*, 29(2):936–945, 2013.

[10] Brice Aubert, Jeremi Regnier, Stephane Caux, and Dominique Alejo. Kalman-filter-based indicator for online interturn short circuits detection in permanent-magnet synchronous generators. *IEEE Transactions on Industrial Electronics*, 62(3):1921–1930, 2014.

[11] Yaw Nyanteh, Chris Edrington, Sanjeev Srivastava, and David Cartes. Application of artificial intelligence to real-time fault detection in permanent-magnet synchronous machines. *IEEE Transactions on Industry Applications*, 49(3):1205–1214, 2013.

[12] K-H Kim, D-U Choi, B-G Gu, and I-S Jung. Fault model and performance evaluation of an inverter-fed permanent magnet synchronous motor under winding shorted turn and inverter switch open. *IET Electric Power Applications*, 4(4):214–225, 2010.

[13] Arun Gandhi, Timothy Corrigan, and Leila Parsa. Recent advances in modeling and online detection of stator interturn faults in electrical motors. *IEEE Transactions on Industrial Electronics*, 58(5):1564–1575, 2010.

[14] Ilsu Jeong, Byong Jo Hyon, and Kwanghee Nam. Dynamic modeling and control for spmsms with internal turn short fault. *IEEE Transactions on Power Electronics*, 28(7):3495–3508, 2012.

[15] Bon-Gwan Gu, Jun-Hyuk Choi, and In-Soung Jung. Development and analysis of interturn short fault model of pmsms with series and parallel winding connections. *IEEE Transactions on Power Electronics*, 29(4):2016–2026, 2013.

[16] Jewon Lee, Yong-Ju Jeon, Doo-chul Choi, SeungHun Kim, and Sang Woo Kim. Demagnetization fault diagnosis method for pmsm of electric vehicle. In *IECON 2013-39th Annual Conference of the IEEE Industrial Electronics Society*, pages 2709–2713. IEEE, 2013.